Journal of the Korean Crystal Growth and Crystal Technology
Vol. 19, No. 3 (2009) 116-124

Effects of total pressure and gravity level on the physical vapor transport of Hg_2Cl_2-Cl_2 system

Jeong-Gil Choi†, Moo Hyun Kwon* and Geug-Tae Kim

Department of Nano-Bio Chemical Engineering, Hannam University, Taejon 305-811, Korea
**Department of Applied Chemistry, Woosuk University, Wanju-gun 565-701, Korea*

(Received April 20, 2009)
(Accepted May 12, 2009)

Abstract Our computational studies for the physical vapor transport crystal growth of Hg_2Cl_2-Cl_2 system evidence suggests that the PVT growth process exhibits the diffusion-dominated behaviors for aspect ratios more than and equal to 10, which would provide purely diffusive transport conditions adequate to microgravity environments less than $10^{-3}g_0$. Also, the regimes of high temperature difference based on the fixed source temperature of 380°C, where ΔT is relatively large enough for the crystal growth of mercurous chloride, the transport rates do not keep increasing with ΔT but tend to some constant value of 2.12 mole $cm^{-2}s^{-1}$. For the aspect ratios of 5, 10, and 20, the transport rate is directly proportional to the total pressure of the system under consideration. For Ar = 5, the rate is increased by a factor of 2.3 with increasing the total pressure from 403 Torr to 935 Torr, i.e., by a factor of 2.3. For both Ar = 10 and 20, the rate is increased by a factor of 1.25 with increasing the total pressure from 403 Torr to 935 Torr.

Key words Mercurous chloride, Convection, Chloride gas, Physical vapor transport

1. Introduction

Mercurous halide materials are the best materials for applications in acousto-optic and opto-electronic devices such as Bragg cells, X-ray detectors operating at ambient temperature [1]. However, despite of the potential of the materials, their commercial applications remain limited for at least two reasons: (1) the materials have extremely difficulty in purification, (2) because of their easy decomposition before melting and high vapor pressures, mercurous halides cannot be solidified as a single crystal directly from the stoichiometric melt [2-5]. Therefore, these materials can be usually grown by the physical vapor transport (PVT) in closed silica glass ampoules. The mechanism of the PVT process is simple: sublimation-condensation in closed silica glass ampoules in temperature gradient imposed between the source material and the growing crystal. Transport phenomena occurring in the vapor are complex and coupled so that it is difficult to design or control the process accurately. Such complexity and coupling are associated with the inevitable occurrence of convection generated by the interaction of gravity with density gradients arising from temperature and/or concentration gradients. Therefore, for a better and thorough understanding of the crystal growth mechanism by the PVT processes, it requires to investigate the roles of convection occurring in the vapor phase during the PVT processes.

In early work on convection during the physical vapor transport, Markham *et al.* [6] examined the effects of thermal and thermo-solutal convections during the PVT process inside vertical cylindrical enclosures for a time-independent system, and showed that even in the absence of gravity, convection can be present, causing nonuniform concentration gradients. They emphasized the role of geometry in the analysis of the effects of convection.

Nadarajah *et al.* [7] addressed the effects of solutal convection for any significant disparity in the molecular weights of the crystal components and the inert gas. Zhou *et al.* [8] reported that the traditional approach of calculating the mass flux assuming one-dimensional flow for low vapor pressure systems is indeed correct. Three-dimensional numerical modeling improvements on PVT processes have made by Rosenberger *et al.* [9]. Much extensive works of transient flow fields in the PVT processes have performed by Duval [10-14]. Also, generic studies on the role of convection the PVT processes of mercurous halides accompanied various impurities related to gravity levels have reported by Kim *et al.* [15-24].

In this theoretical study, a two-dimensional model is used for the analysis of the PVT processes during vapor-growth of mercurous chloride crystals (Hg_2Cl_2) in

†Corresponding author
Tel: +82-42-629-8841
Fax: +82-42-629-8835
E-mail: jgchoi@hnu.kr

horizontally oriented, cylindrical, closed ampoules in a two-zone furnace system. Thermally buoyancy-driven convection will be considered at this point, primarily for a mixture of Hg_2Cl_2 vapor and impurity of chloride gas (Cl_2), although solutally-induced convection is more important than thermal convection in some cases. It is the purpose of this paper to relate applied solutal convection process parameters such as such (1) total pressures, (2) temperature differences between the source and the crystal region, (3) gravitational levels, and (4) binary diffusivity coefficients to the crystal growth rate and the maximum velocity magnitude, in order to examine the effects of the presence of chloride gas (Cl_2) on solutal buoyancy-driven convection in order to gain insights into the underlying physicochemical processes.

2. Physical and Mathematical Formulations

Consider a rectangular enclosure of height H and transport length L, shown in Fig. 1. The source is maintained at a temperature T_s, while the growing crystal is at a temperature T_c, with $T_s > T_c$. PVT of the transported component A (Hg_2Cl_2) occurs inevitably, due to presence of impurities, with the presence of a component B (Cl_2). The interfaces are assumed to be flat for simplicity. Thermodynamic equilibria are assumed at the interfaces so that the mass fractions at the interfaces are kept constant at $\omega_{A,s}$ and $\omega_{A,c}$. On the vertical non-reacting walls appropriate velocity boundary conditions are no-slip, the normal concentration gradients are zero, and wall temperatures are imposed as nonlinear temperature gradients. Thermo-physical properties of the fluid are assumed to be constant, except for the density. The density is assumed to be a function of both temperature and concentration. The ideal gas law and Dalton's law of partial pressures are used.

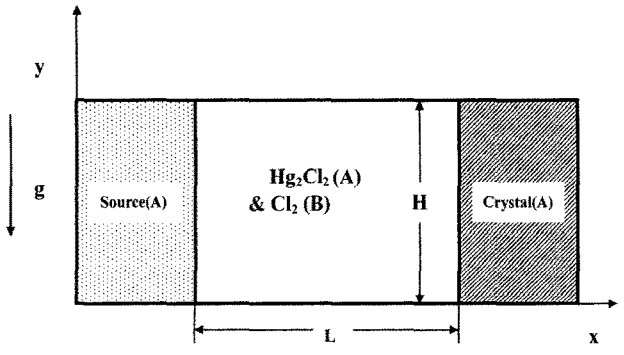

Fig. 1. Schematic of PVT growth reactor in a two-dimensional rectangular system.

The transport of fluid within a rectangular PVT crystal growth reactor is governed by a system of elliptic, coupled conservation equations for mass (continuity), momentum, energy and species (diffusion) with their appropriate boundary conditions. Let u_x, u_y denote the velocity components along the x- and y-coordinates in the x, y rectangular coordinate, and let T, ω_A, p denote the temperature, mass fraction of species A (Hg_2Cl_2) and pressure, respectively.

The dimensionless variables are defined as follows:

$$x^* = \frac{x}{H},\ y^* = \frac{y}{H}, \tag{1}$$

$$u^* = \frac{u_x}{U_c},\ v^* = \frac{u_y}{U_c},\ p^* = \frac{p}{\rho_c U_c^2}, \tag{2}$$

$$T^* = \frac{T - T_c}{T_s - T_c},\ \omega_A^* = \frac{\omega_A - \omega_{A,c}}{\omega_{A,s} - \omega_{A,c}}. \tag{3}$$

The dimensionless governing equations are given by:

$$\nabla^* \bullet V^* = 0, \tag{4}$$

$$\vec{V}^* \bullet \nabla^* \vec{V}^* = -\nabla^* p^* + Pr \cdot Ar \nabla^{*2} \vec{V}^* - \frac{Ra \cdot Pr}{Ar} \cdot T^* \cdot e_g, \tag{5}$$

$$\vec{V}^* \bullet \nabla^* T^* = Ar \nabla^{*2} T^* \tag{6}$$

$$\vec{V}^* \bullet \nabla^* \omega_A^* = \frac{Ar}{Le} \nabla^{*2} \omega_A^* \tag{7}$$

These nonlinear, coupled sets of equations are numerically integrated with the following boundary conditions:

On the walls ($0 < x^* < Ar$, $y^* = 0$ and 1):

$$u^*(x^*,0) = u^*(x^*,1) = v^*(x^*,0) = v^*(x^*,1) = 0 \tag{8}$$

$$\frac{\partial \omega_A^*(x^*,0)}{\partial y^*} = \frac{\partial \omega_A^*(x^*,1)}{\partial y^*} = 0,$$

$$T^*(x^*,0) = T^*(x^*,1) = \frac{T - T_c}{T_s - T_c}$$

On the source ($x^* = 0$, $0 < y^* < 1$):

$$u^*(0,y^*) = -\frac{Ar}{Le(1 - \omega_{A,s})} \frac{\Delta\omega}{\partial x^*} \frac{\partial \omega_A^*(0,y^*)}{\partial x^*}, \tag{9}$$

$$v^*(0,y^*) = 0,$$

$$T^*(0,y^*) = 1,$$

$$\omega_A^*(0,y^*) = 1.$$

On the crystal ($x^* = Ar$, $0 < y^* < 1$):

$$u^*(Ar,y^*) = -\frac{Ar}{Le(1 - \omega_{A,c})} \frac{\Delta\omega}{\partial x^*} \frac{\partial \omega_A^*(Ar,y^*)}{\partial x^*}, \tag{10}$$

$$v^*(Ar,y^*) = 0,$$
$$T^*(Ar,y^*) = 0,$$
$$\omega_A^*(Ar,y^*) = 0.$$

Interfacial velocities (sublimation and condensation velocities) in Eqs. (9) and (10) can also be expressed in terms of a dimensionless Peclet number and a concentration parameter as follows:

$$u(0,y^*) = -\frac{1}{Pe(C_v - 1)}\frac{\partial \omega_A^*(0,y^*)}{\partial x^*} \quad (11)$$

$$u(Ar,y^*) = -\frac{\Delta\omega}{PeC_v}\frac{\partial \omega_A^*(Ar,y^*)}{\partial x^*} \quad (12)$$

where the Peclet number and concentration parameter C_v are defined as

$$Pe = \frac{U_{adv}L}{D_{AB}},\ C_v = \frac{1 - \omega_{A,c}}{\Delta\omega}. \quad (13)$$

The Peclet number can be also estimated by thermodynamic variables:

$$Pe = \ln\left(\frac{p_B(L)}{p_B(0)}\right). \quad (14)$$

U_{adv} is a characteristic velocity which depends on the thermodynamics of PVT processes, i.e., the vapor pressure of Hg_2Cl_2 as a function of temperature. The mass fraction at the solid-vapor interfaces is fixed at the corresponding temperature. Thus for a given set of conditions, the mass fraction cannot be varied independently. The concentration parameter C_v in Eqs. (11) and (12) represents the ratio of mass fraction.

In the dimensionless parameters in the governing equations the thermo-physical properties of the gas mixture are estimated from gas kinetic theory using Chapman-Enskog's formulas [25], refer to appendix attached.

The partial pressure (in the unit of Pascal) of Hg_2Cl_2 is given by Duval as [10]

$$p_A = e^{(a - b/T)}. \quad (15)$$

where the constants a and b are 29.75 and b = 11767.1, respectively.

3. Results and Discussion

The purposes for this study is to correlate the growth rate and the convective intensity, i.e., $|U|_{max}$, the maximum magnitude of velocity vector, to process parameters such as (1) total pressures, (2) temperature differences between the source and the crystal region, (3) gravitational levels, and (4) binary diffusivity coefficients. It is desirable to express some results in terms of dimensional growth rate, however they are also applicable to parameter ranges over which the process varies in the manner given. The six dimensionless parameters, namely Gr, Ar, Pr, Le, C_v and Pe, are independent and

Table 1
Typical thermo-physical properties used in this study (M_A = 472.086, M_B = 70.91)

Transport length, L	10 cm
Height, H	2 cm
Source temperature, T_s	380°C
Crystal temperature, T_c	290°C
Thermal diffusivity, α	0.098 cm^2/s
Kinematic viscosity, ν	0.084 cm^2/s
Diffusivity, D_{AB}	0.101 cm^2/s
Prandtl number, Pr	0.85
Lewis number, Le	0.97
Peclet, Pe	6.10
Concentration number, C_v	1.00
Total system pressure, P_T	935 Torr
Partial pressure of component B, P_B	10 Torr
Thermal Grashof number, Gr	1.50×10^5
Solutal Grashof number, Gr_s	1.24×10^6

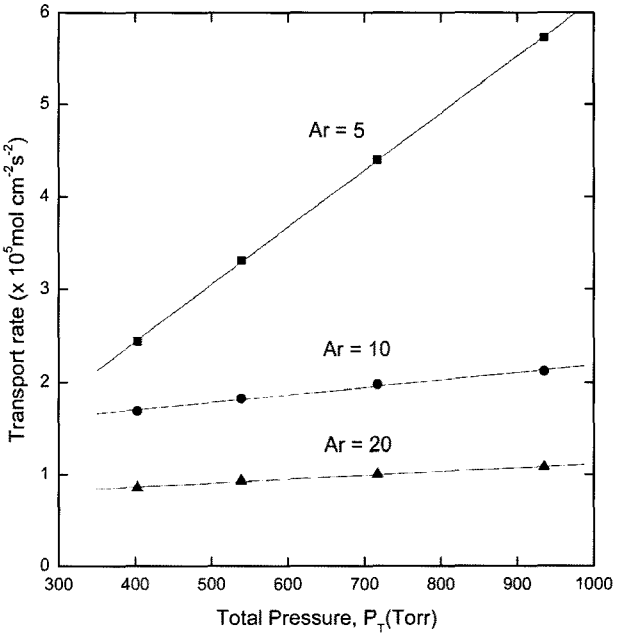

Fig. 2. Transport rate of as a function of total pressure at different aspect ratios (Ar = 5, 10, 20) and different temperatures of the source and crystal ends (T_s = 380°C, T_c = 290°C; T_s = 370°C, T_c = 280°C; T_s = 360°C, T_c = 270°C; T_s = 350°C, T_c = 260°C) with fixed temperature difference (ΔT = 90 K) between the source and the crystal region, for a horizontal ampoule with a linear wall temperature profile, and $g_y = 1g_0$.

arise naturally from the dimensionless governing equations and boundary conditions. Typical dimensionless parameters and physical properties for the operating conditions of this study are shown in Table 1. In this study, because the molecular weight of the chloride gas (Cl_2) is not equal to that of the crystal component (Hg_2Cl_2) during the physical vapor transport, solutal effects only should be considered.

Fig. 2 shows the transport rate of as a function of total pressure at different aspect ratios (Ar = 5, 10, 20) and $\Delta T = 90$ K, for a horizontal ampoule with linear wall temperature profile, and $g_y = 1g_0$. The four cases of different source and crystal temperatures are as follows: $T_s = 380°C$, $T_c = 290°C$; $T_s = 370°C$, $T_c = 280°C$; $T_s = 360°C$, $T_c = 270°C$; $T_s = 350°C$, $T_c = 260°C$. All of the cases for the temperature difference between the source and the crystal region are same, i.e., 90 K. For the aspect ratios of 5, 10, and 20, the transport rate is directly proportional to the total pressure of the system under consideration. For Ar = 5, the rate is increased by a factor of 2.3 with increasing the total pressure from 403 Torr to 935 Torr, i.e., by a factor of 2.3. Its gradient is 618×10^{-5} mole cm^{-2} s^{-1} $Torr^{-1}$. On the other hand, the gradients for Ar = 10 and 20 are 80.8 and 41.3×10^{-5} mole cm^{-2} s^{-1} $Torr^{-1}$, respectively. For both Ar = 10 and 20, the rate is increased by a factor of 1.25 with increasing the total pressure from 403 Torr to 935 Torr. For more than aspect ratios of 10, the corresponding rates have the same increasing factor of 1.25, indicative of same dependence of total pressure. It is also found that as the aspect ratio increases, the rate is decreases by a factor of about 0.18, i.e., one fifth in reduction, which is likely to be due to the effects of side walls. Fig. 3 shows the relationship between the maximum magnitude of velocity vector, $|U|_{max}$ (cm s^{-1}) and a total pressure at three different aspect ratios of 5, 10 and 20, corresponding to Fig. 2. As shown in Fig. 3, with increasing the total pressure, the $|U|_{max}$ first-order exponentially decays for Ar = 10 and increases for Ar = 20. It reflects the convection-dominated mode for Ar = 5 and diffusion-dominated for both Ar = 10 and 20. Thus, the effects of sidewalls transits the convection flow fields to the diffusion mode, as confirmed through the effects of zero-gravity in Fig. 12 later. Fig. 4 shows the relationship between the dimensionless solutal Grashof number, Gr_s and the total pressure, P_T for Ar = 5 and 10 with the same temperature difference, $\Delta T = 90$ K. With increasing total pressures, the corresponding solutal Grashof numbers for Ar = 5 are significantly varied in comparison with Ar = 10.

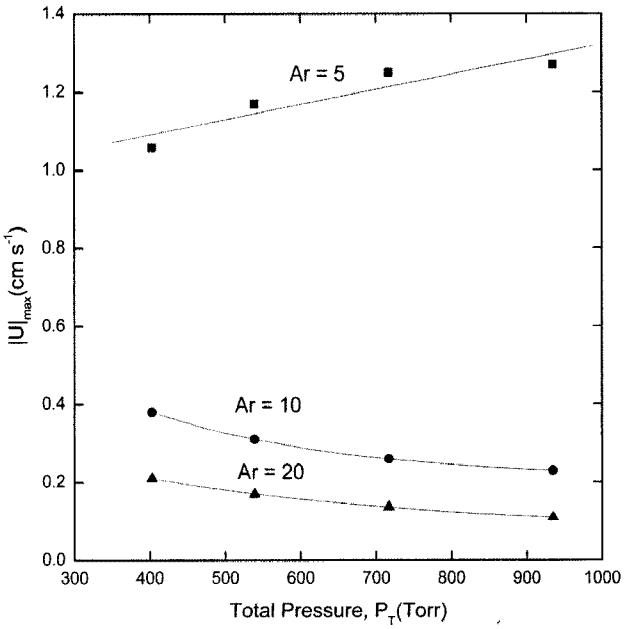

Fig. 3. The maximum magnitude of velocity vector, $|U|_{max}$ (cm s^{-1}) of as a function of total pressure at different aspect ratios of 5, 10 and 20, corresponding to Fig. 2.

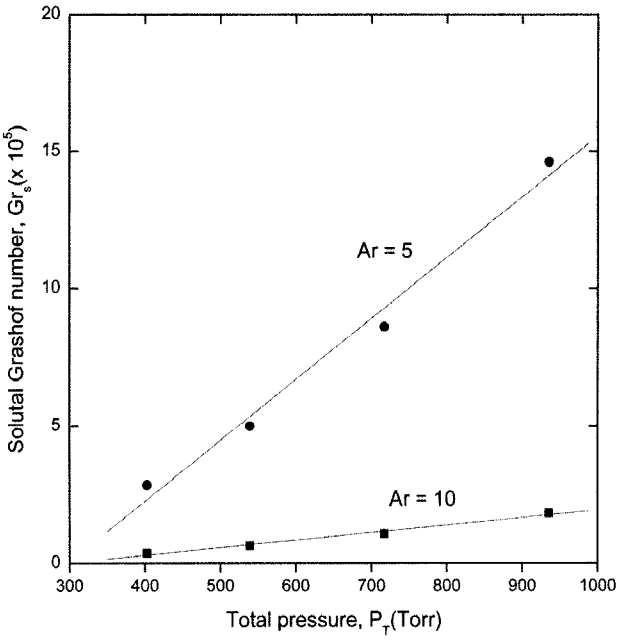

Fig. 4. The relationship between the dimensionless solutal Grashof number, Gr_s and the total pressure, P_T for Ar = 5 and 10 with the same temperature difference, $\Delta T = 90$ K.

Fig. 5 shows the relationship between the binary diffusivity coefficient, D_{AB} (cm^2 s^{-1}) and the total pressure for Ar = 10 and $\Delta T = 90$ K. As shown in Fig. 5, $D_{AB} \sim 1/P_T$ so that it is confirmed the binary diffusivity coefficients at Ar = 10 and $\Delta T = 90$ K are inversely proportional to the total pressures of the system. Consequently, a decrease in the binary diffusivity coefficient results in

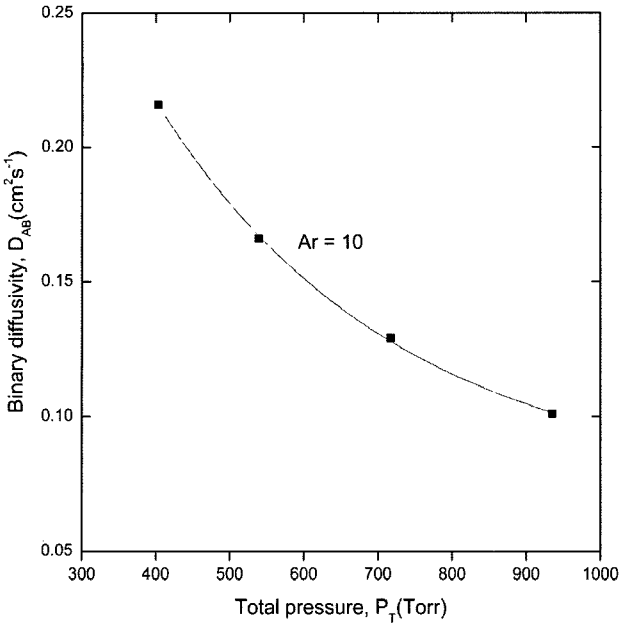

Fig. 5. The link between the binary diffusivity coefficient, D_{AB} (cm^2 s^{-1}) and the total pressure for Ar = 10 and ΔT = 90 K.

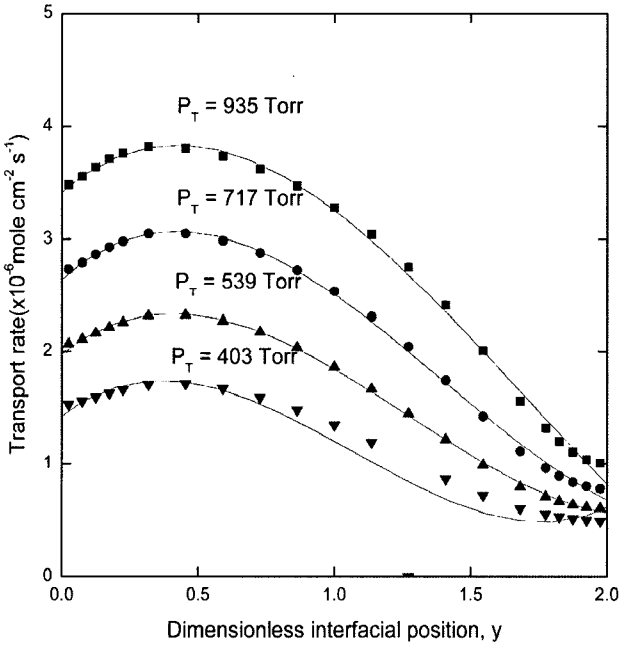

Fig. 6. Interfacial distribution of transport rates along the y-direction of the crystal surface at different aspect ratios of 5, 10 and 20 for a horizontal ampoule with a linear wall temperature profile, $g_y = 1g_0$, and Ar = 5.

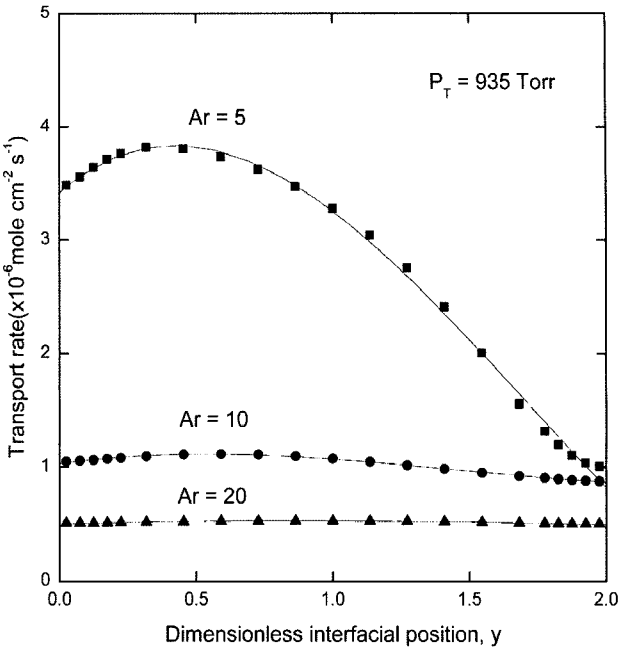

Fig. 7. Interfacial distribution of transport rates along the y-direction of the crystal surface at different aspect ratios of 5, 10 and 20, for a horizontal ampoule with a linear wall temperature profile, $g_y = 1g_0$, and P_T = 935 Torr.

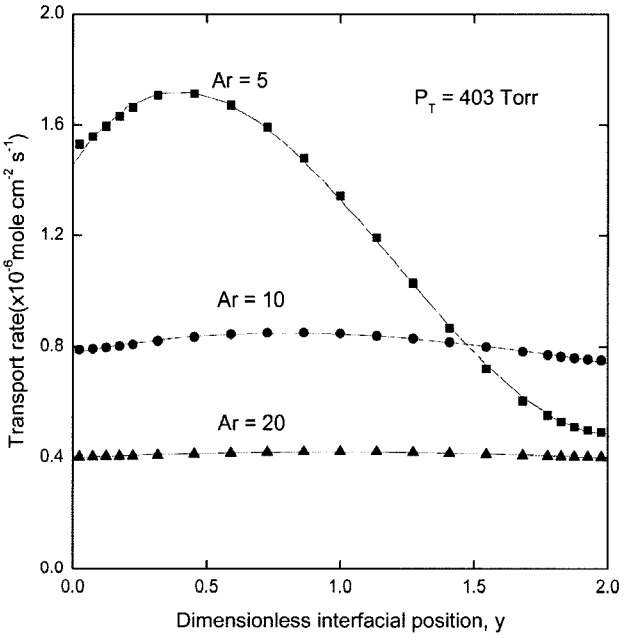

Fig. 8. Interfacial distribution of transport rates along the y-direction of the crystal surface at different aspect ratios of 5, 10 and 20 for a horizontal ampoule with a linear wall temperature profile, $g_y = 1g_0$, and P_T = 403 Torr.

an increase in the total pressure of the system so that the corresponding transport rate would be increased. Fig. 6 shows the interfacial distribution of transport rates along the y-direction of the crystal surface at different total pressures for a horizontal ampoule with a linear wall temperature profile, $g_y = 1g_0$, and Ar = 5. The maximum rates appear at the neighborhood of dimensionless interfacial position, y = 0.5 for all cases, shown in Fig. 6. Variations in the transport rate are dependent on the total pressure, and are reduced and converged at a value of 1 near at the dimensionless interfacial position of 2.0. Variation at the maximum rate is directly

and linearly related to the total pressure of Ar = 5. Fig. 7 shows the interfacial distribution of transport rates along the y-direction of the crystal surface at different aspect ratios of 5, 10 and 20, for a horizontal ampoule with a linear wall temperature profile, $g_y = 1g_0$, and P_T = 935 Torr. The maximum transport rate for Ar = 5 appears at the dimensionless interfacial position of 0.5. The deviations between the maximum and the minimum rates for both Ar = 10 and 20 remain nearly invariant, which is likely to be due to the diffusion-dominated mode. Fig. 8 shows the interfacial distribution of transport rates for the system as Fig. 7, except for P_T = 403 Torr. The maximum rate increases with decreasing the aspect ratio. The minimum rate for Ar = 5 is smaller than for Ar = 10, but greater than for Ar = 20. This finding is likely to be due to the interactions between the effects of side walls and convection, which would be switched from the convection to the diffusion-dominated mode. As shown in Fig. 8, the profiles of transport rates for Ar = 10 and 20 exhibit flat pattern, which indicates the diffusion-dominated regimes during the physical vapor transport processes. In other words, the mass transport rates could be mainly classified as two regimes: the flatter part at high aspect ratios, i.e., the diffusion-dominated; the steeper part at relatively low aspect ratios, the circulatory convection-dominated regime. Therefore, from Figs. 6 through 8, such rate profiles show a steeper convective flow field near at the dimensionless interfacial position of 0.5 and predict the asymmetry of the convective flow fields. As pointed out by Rosenberger *et al.* [9], high fidelity modeling of PVT processes requires full account of the three dimensional flow in the ampoule adequate for the prediction of the crystal growth rates.

Fig. 9 shows the transport rate of as a function of temperature difference between the source and crystal ends for two cases of the fixed source and crystal temperatures, with a horizontal ampoule of aspect ratio of 10 and a linear wall temperature profile, and $g_y = 1g_0$. Two profiles of transport rates versus the temperature difference between the source and the crystal end are based on the fixed source temperature of 380°C and the fixed crystal temperature of 290°C. For $20\ K \le \Delta T \le 80\ K$, the rate for the fixed source temperature of 380°C is varied slowly, and the variations in the rate are nearly negligible for $40\ K \le \Delta T \le 80\ K$. In other words, the regimes of high temperature difference based on the fixed source temperature of 380°C, where ΔT is relatively large enough for the crystal growth of mercurous chloride, the transport rates do not keep increasing with ΔT but tend to some constant value of 2.12 mole $cm^{-2}s^{-1}$. On the other hand, the rate for the fixed source temperature of 290°C varies linearly and directly with the temperature difference for the temperature ranges under consideration.

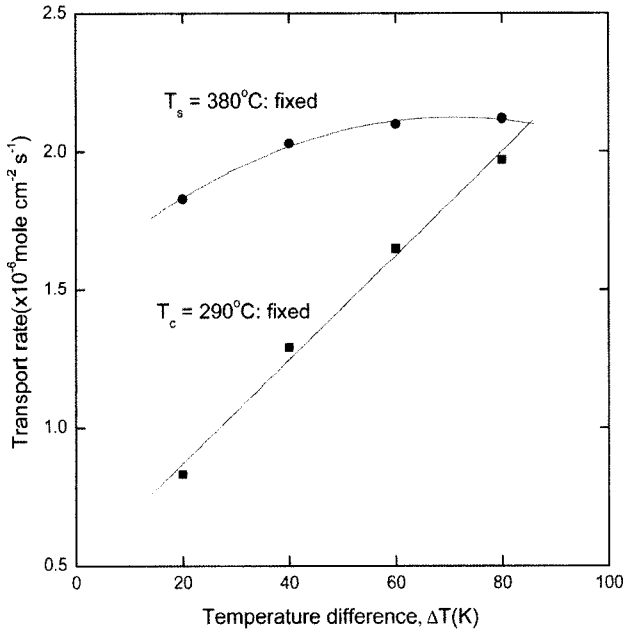

Fig. 9. Transport rate of as a function of temperature difference between the source and crystal ends for two cases of the fixed source and crystal temperatures, with a horizontal ampoule of aspect ratio of 10 and a linear wall temperature profile, and $g_y = 1g_0$.

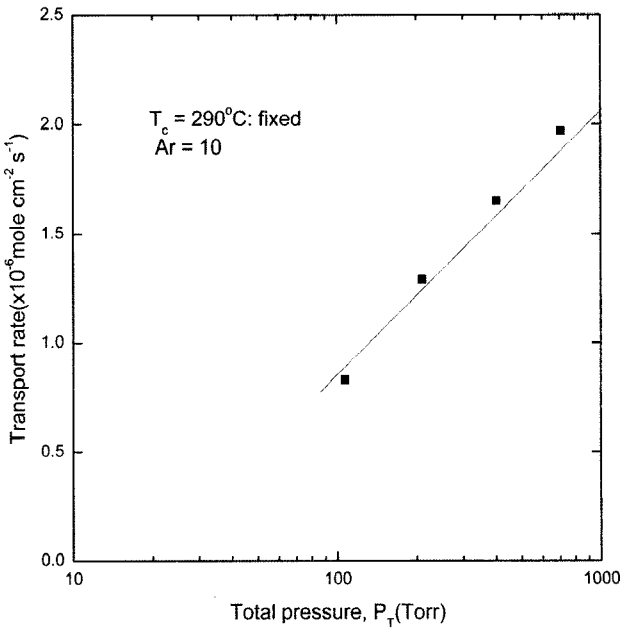

Fig. 10. Transport rate of as a function of a total pressure for the fixed crystal temperature of 290°C, with a horizontal ampoule of aspect ratio of 10 and a linear wall temperature profile, and $g_y = 1g_0$.

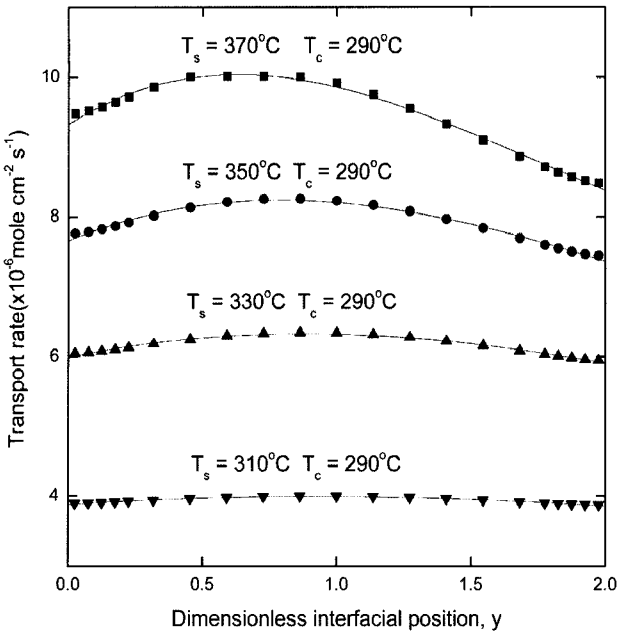

Fig. 11. Transport rate of as a function of a total pressure for the fixed crystal temperature of 290°C, with a horizontal ampoule of aspect ratio of 10 and a linear wall temperature profile, and $g_y = 1g_0$.

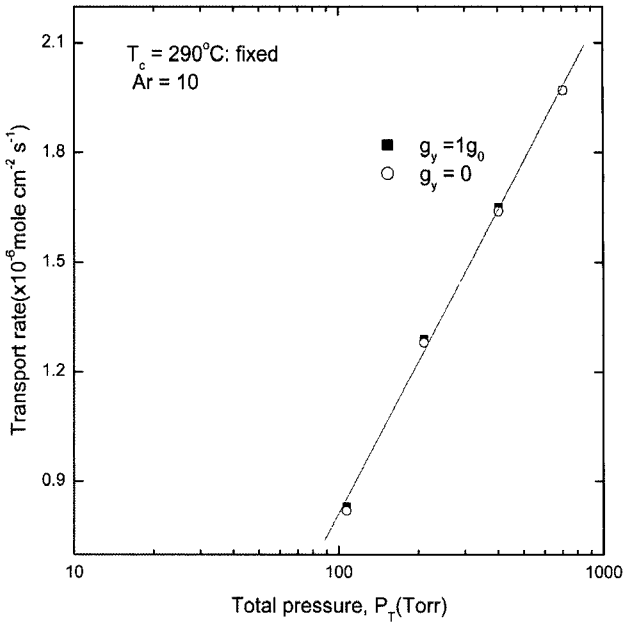

Fig. 12. The effects of gravity level on transport rate versus total pressure for the fixed crystal temperature of 290°C, a horizontal ampoule of aspect ratio of 10 and a linear wall temperature profile.

Fig. 10 shows the transport rate of as a function of total pressure for the fixed crystal temperature of 290°C, with a horizontal ampoule of aspect ratio of 10 and a linear wall temperature profile, and $g_y = 1g_0$. The transport rate shows a logarithm linear relation with the total pressure of the system. This implies the transport rate is significantly dependent on the total pressure under consideration. Fig. 11 shows the transport rate of as a function of total pressure for the fixed crystal temperature of 290°C, with a horizontal ampoule of aspect ratio of 10 and a linear wall temperature profile, and $g_y = 1g_0$. As the temperature difference between the source and the crystal end increases form 20 K up to 80 K, the variations between the maximums and the minimum transport rates are increased gradually. The maximum rates occur at the dimensionless interfacial position of 0.5. For the case of $T_s = 310°C$ and $T_c = 290°C$, the corresponding interfacial distribution profile approaches the flatness.

Fig. 12 shows the effects of gravity level on transport rate versus total pressure for the fixed crystal temperature of 290°C, a horizontal ampoule of aspect ratio of 10 and a linear wall temperature profile. The dependences of the rate on total pressure at zero gravity could be achieved by keeping all other conditions same, except the gravity term. As shown in Fig. 12, it is clear that the transport rates for Ar = 10 versus the total pressure are independent on the gravity level, because the rates between the $g = 1g_0$ and zero-gravity are nearly same, which indicates the diffusion mode is predominant. Consequently, the convective effects can easily be suppressed in physical vapor transport systems for aspect ratios more than and equal to Ar = 10, i.e. at 10 and 20.

4. Conclusions

The effects of total pressure and gravity level on convection have investigated by changing the aspect ratio (transport length-to-width) and the temperature difference between the source and the crystal regime for the physical vapor transport crystal growth of Hg_2Cl_2-Cl_2 system. Because of the change of aspect ratio and the temperature difference, different solutal Grashof number and hence different convective conditions could be achieved in the crystal gorwth of mercurous chloride by the physical vapor transport processes. Our computation modeling evidence suggests that the PVT growth process exhibits the diffusion-dominated behaviors for aspect ratios more than and equal to 10, which would provide purely diffusive transport conditions adequate to microgravity environments less than $10^{-3}g_0$. It is found that there is no difference in the transport rate between the ground based and zero gravity conditions. Also, the regimes of high temperature difference based on the

fixed source temperature of 380°C, where ΔT is relatively large enough for the crystal growth of mercurous chloride, the transport rates do not keep increasing with ΔT but tend to some constant value of 2.12 mole $cm^{-2}s^{-1}$. For the aspect ratios of 5, 10, and 20, the transport rate is directly proportional to the total pressure of the system under consideration. For Ar = 5, the rate is increased by a factor of 2.3 with increasing the total pressure from 403 Torr to 935 Torr, i.e., by a factor of 2.3. For both Ar = 10 and 20, the rate is increased by a factor of 1.25 with increasing the total pressure from 403 Torr to 935 Torr. For more than aspect ratios of 10, the corresponding rates have the same increasing factor of 1.25, indicative of same dependence of total pressure. It is also found that as the aspect ratio increases, the rate is decreases by a factor of about 0.18, i.e., one fifth in reduction, which is likely to be due to the effects of side walls.

Acknowledgement

This paper has been supported by the 2009 Hannam University Research Fund (March 1, 2009 through February 28, 2010).

References

[1] N.B. Singh, M. Gottlieb, G.B. Brandt, A.M. Stewart, R. Mazelsky and M.E. Glicksman, "Growth and characterization of mercurous halide crystals: mercurous bromide system", J. Crystal Growth 137 (1994) 155.

[2] N.B. Singh, R.H. Hopkins, R. Mazelsky and J.J. Conroy, "Purification and growth of mercurous chloride single crystals", J. Crystal Growth 75 (1970) 173.

[3] J.-S. Kim, Sudhir B. Trivedi, Jolanta Soos, Neelam Gupta and Witold Palosz, "Growth of Hg_2Cl_2 and Hg_2Br_2 single crystals by physical vapor transport", J. Crystal Growth 310 (2008) 2457.

[4] S.J. Yosim and S.W. Mayer, "The mercury-mercuric chloride system", J. Phys. Chem. 60 (1960) 909.

[5] N.B. Singh, M. Gottlieb, A.P. Goutzoulis, R.H. Hopkins and R. Mazelsky, "Mercurous Bromide acousto-optic devices", J. Crystal Growth 89 (1988) 527.

[6] B.L. Markham, D.W. Greenwell and F. Rosenberger, "Numerical modeling of diffusive-convective physical vapor transport in cylindrical vertical ampoules", J. Crystal Growth 51 (1981) 426.

[7] A. Nadarajah, F. Rosenberger and J. Alexander, "Effects of buoyancy-driven flow and thermal boundary conditions on physical vapor transport", J. Crystal Growth 118 (1992) 49.

[8] H. Zhou, A. Zebib, S. Trivedi and W.M.B. Duval, "Physical vapor transport of zinc-telluride by dissociative sublimation", J. Crystal Growth 167 (1996) 534.

[9] F. Rosenberger, J. Ouazzani, I. Viohl and N. Buchan, "Physical vapor transport revised", J. Crystal Growth 171 (1997) 270.

[10] W.M.B. Duval, "Convection in the physical vapor transport process-- I: Thermal", J. Chemical Vapor Deposition 2 (1994) 188.

[11] W.M.B. Duval, "Convection in the physical vapor transport process-- II: Thermosolutal convection", J. Chem. Vapor Deposition, 2 (1994b), 282.

[12] W.M.B. Duval, "Transition to chaos in the physical vapor transport process--I: fluid mechanics problem phenomena in microgravity", Fluids Eng. Div. ASME 175 (1993) 51.

[13] W.M.B. Duval, N.E. Glicksman and B. Singh, "Physical vapor transport of mercurous chloride crystals; design of a microgravity experiment", J. Crystal Growth 174 (1997) 120.

[14] P.A. Tebbe, S.K. Loyalka and W.M.B. Duval, "Finite element modeling of asymmetric and transient flow flieds during physical vapor transport", Finite Elements in Analysis and Design 40 (2004) 1499.

[15] G.T. Kim, W.M.B. Duval, N.B. Singh and M.E. Glicksman "Thermal convective effects on physcial vapor transport growth of mercurous chloride crystals (Hg_2C1_2) for axisymmetric 2-D cylindrical enclosure", Modelling. Simul. Mater. Sci. Eng. 3 (1995) 331.

[16] G.T. Kim, W.M.B. Duval and M.E. Glicksman "Thermal convection in physical vapour transport of mercurous chloride (Hg_2Cl_2) for rectangular enclosures", Modelling. Simul. Mater. Sci. Eng. 5 (1997) 289.

[17] G.T. Kim, W.M.B. Duval and M.E. Glicksman "Effects of asymmetric temperature profiles on thermal convection during physical vapor transport of Hg_2Cl_2", Chem. Eng. Comm. 162 (1997) 45.

[18] J.-G. Choi, K.-H. Lee, M.-H. Kwon and G.-T. Kim, "Effect of accelerational perturbations on physical vapor transport crystal growth under microgravity environments", J. Korean Crystal Growth and Crystal Technology 16 (2006) 203.

[19] G.-T. Kim and K.-H. Lee, "Parametric studies on convection during the physical vapor transport of mercurous chloride (Hg_2Cl_2)", J. Korean Crystal Growth and Crystal Technology 14 (2004) 281.

[20] G.T. Kim, "Convective-diffusive transport in mercurous chloride (Hg_2Cl_2) crystal growth", J. Ceramic Processing Research 6 (2005) 110.

[21] J.-G. Choi, K.-H. Lee and G.-T. Kim, "Effects of inert gas (Ne) on thermal convection of mercurous chloride system of Hg_2Cl_2 and Ne during physical vapor transport", J. Korean Crystal Growth and Crystal Technology 18 (2008) 225.

[22] J.-G. Choi, K.-H. Lee and G.-T. Kim, "Generic studies on thermo-solutal convection of mercurous chloride system of Hg_2Cl_2 and Ne during physical vapor transport", J. Korean Crystal Growth and Crystal Technology 1 (2009) 39.

[23] M.H. Kwon and G.-T. Kim, "Theoretical gravity studies on roles of convection in crystal growth of Hg_2Cl_2-Xe by physical vapor transport under normal and high grav-

ity environments", submitted to J. Korean Crystal Growth and Crystal Technology (2009).
[24] M.H. Kwon and G-T. Kim, "Effects of nonlinear temperature profiles and microgravity environments on physical vapor transport of Hg_2Cl_2-Xe system", submitted to J. Korean Crystal Growth and Crystal Technology (2009).
[25] R.B. Bird, W.E. Stewart and E.N. Lightfoot, "Transport phenomena" (John Wiley and Sons, New York, NY, 1960).